arXiv:cond-mat/0407391v1 [cond-mat.soft] 15 Jul 2004

Short chains at solid surfaces: wetting transition from a density functional approach

P. Bryk and S. Sokołowski
Department for the Modeling of Physico-Chemical Processes,
Maria Curie-Skłodowska University, 20-031 Lublin, Poland

A microscopic density functional theory is used to investigate the adsorption of short chains on attractive solid surfaces. We analyze the structure of the adsorbed fluid and investigate how the wetting transition changes with the change of the chain length and with relative strength of the fluid-solid interaction. End segments adsorb preferentially in the first adsorbed layer whereas the concentration of the middle segments is enhanced in the second layer. We observe that the wetting temperature rescaled by the bulk critical temperature decreases with an increase of the chain length. For longer chains this temperature reaches a plateau. For the surface critical temperature an inverse effect is observed, i.e. the surface critical temperature increases with the chain length and then attains a plateau. These findings may serve as a quick estimate of the wetting and surface critical temperatures for fluids of longer chain lengths.

I. INTRODUCTION

Alkanes are often used as standard substances in studies of wetting and adhesion. This is connected with the industrial importance of these chemicals, being major constituents of fuels, oils and lubricants. Consequently, the literature aiming at theoretical description of adsorption of chain particles is very rich – see for the review Refs.[1,2]. Among different theoretical approaches based on application of lattice-off models, three groups of methods are of a particular importance. These are computer simulation techniques,[1,3,4], the self-consistent field theory calculations[2,5,6] and the approaches based on the applications of different versions of density functional theory (DFT)[7,8,9,10,11,12,13,14,15,16,17].

In recent years there have been proposed several density functional approaches for molecular systems. One of the earliest density functional-based studies were carried out by Woodward[8,9] more than ten years ago. Next, Yethiraj and Woodward[10,11] proposed a theory that combined a single-chain Monte Carlo simulation and a DFT scheme. Another class of density functional methods was based on on the interaction site formalism of Chandler et al.[12,13]. Finally, we should mention about theories which extends Wertheim's thermodynamic perturbation theory[18] to the case of nonuniform chain fluids[16,17]. From computational point of view the latter theories, especially the theory of Yu and Wu[17,19], seem to be particularly convenient to study the structure and thermodynamic properties of nonuniform fluids composed of tangentially bonded chains.

Majority of previous density-functional based studies of adsorption of chain particles have considered models with repulsive forces only and have been devoted to study of the packing of hard chains at hard walls cf. eg.[8,9,10,13,16,17,20]. More recently theoretical effort has been shifted towards studies of systems with attractive interparticle and particle-wall forces[21,22,23,24,25,26]. Particularly worth to notice is the recent publication of Müller et al.[23,25], who have reported the results of Monte Carlo, density functional and self-consistent field theory investigations of surface and interfacial properties of a molecular fluid composed a short linear chains (built of 10 segments). Their approach has been based on a model, according to which the molecules are treated as spherical sites connected by springs and with site interacting with other sites and with the surface via Lennard-Jones type potentials. Wertheim's thermodynamic perturbation theory has been applied to model connectivity of the segments. They have found[25] that for the theory to be accurate, it is important to decompose the free energy into repulsive and attractive contributions with different approximations (e.g. different weighted densities) for the two parts. The developed approach has been able to reproduce the results of computer simulations with a good accuracy. However, it also requires much of computational effort. Consequently, extensive studies of surface phase transitions within the framework of the theory of Müller et al.[25] would be rather time-consuming. In our opinion an attractive alternative for performing such studies provides theory of Yu and Wu[17,19].

In this work we apply the density functional theory of Yu and Wu[17,19] to study adsorption of molecules built of freely jointed tangent Lennard-Jones segments on a solid surface. The main purpose of our work is to investigate the wetting transition for short chains built of from 2 up to 10 identical segments. A mean-field approximation is applied to calculate the contribution to the free energy functional arising form segment-segment interaction. Therefore we do not expect our theoretical predictions to remain in a quantitative agreement with computer simulations. However, we can expect that a general picture of the wetting phenomena in such systems should be correctly predicted at a qualitative level.

The evaluations of surface phase diagrams requires the knowledge of the bulk phase diagrams for the fluids in question. Numerous calculations of the bulk thermodynamic properties for models similar to that applied here have been reported in the literature, see e.g.[25,27,28,29,30,31] However, despite this similarity, there also exist several

differences, which lead to differences in the course of the liquid-vapor coexistence envelope. Therefore our surface calculations are preceded by the study aiming at the evaluation of the bulk phase equilibria.

II. THEORY

We consider a fluid of chain particles in contact with an impenetrable solid surface. Each individual particle of the fluid is composed of M spherical segments. Although the theory can be written down for a quite general case in which the chain may consist of segments of different sizes, through this work we restrict ourselves to the case of the segments of identical diameters σ. The segments are tangentially jointed by a bonding potential acting between the adjacent segments of the same chain. The total bonding potential $V_b(\mathbf{R})$ is a sum of bonding potentials v_b between the segments

$$V_b(\mathbf{R}) = \sum_{j=1}^{M-1} v_b(|\mathbf{r}_{j+1} - \mathbf{r}_j|) \; . \tag{1}$$

where $\mathbf{R} \equiv (\mathbf{r}_1, \mathbf{r}_2, \cdots, \mathbf{r}_M)$ denotes a set of coordinates describing the segment positions. According to our treatment this potential satisfies the relation

$$\exp[-\beta V_b(\mathbf{R})] = \prod_{j=1}^{M-1} \delta(|\mathbf{r}_{j+1} - \mathbf{r}_j| - \sigma)/4\pi\sigma^2 \; . \tag{2}$$

Note that the model used here differs from those applied in Refs.[2,23,25,28], where the so-called finitely extensible nonlinear elastic potential, responsible for the connectivity between the adjacent segments has been employed. In our approach we assume that the bonding potential, v_b, is of infinitely short range.

The fluid is in contact with a solid surface and each segment j interacts with the surface via a Lennard-Jones (9-3) potential

$$v_j(z_j) = \varepsilon_{gs} \left[(z_0/z_j)^9 - (z_0/z_j)^3 \right] , \tag{3}$$

where z_j is the distance between the segment j and the surface. The energy parameter, ε_{gs}, and distance parameter, z_0, are the same for all the segments.

Similar to previous studies[17,20] we assume that the segments have a hard core forbidding any configuration that would lead to an overlap between two segments. An additional pair-wise attractive interaction between the segments is imposed. This attractive potential between two segments separated by the distance r is

$$u(r) = \begin{cases} 0 & \text{for} \;\; r \le \sigma, \\ 4\varepsilon \left[(\sigma/r)^{12} - (\sigma/r)^6 \right] & \text{for} \;\; \sigma < r \le r_{cut}, \\ 0 & \text{for} \;\; r > r_{cut}, \end{cases} \; . \tag{4}$$

In the above r_{cut} is the cut-off distance, and we have set its value to 3σ. The energy parameter ε is independent of the interacting segment index. The form of the potential (4) excludes the interaction between the adjacent segments within the same chain.

Within the framework of the theory of Yu and Wu[17] the grand potential of the system Ω is defined as a functional of the local density of the fluid, $\rho(\mathbf{R})$,

$$\Omega[\rho(\mathbf{R})] = F_{id}[\rho(\mathbf{R})] + F_{ex}[\rho(\mathbf{R})] + \int d\mathbf{R}\rho(\mathbf{R})(V_{ext}(\mathbf{R}) - \mu) + F_{att}[\rho(\mathbf{R})] \; , \tag{5}$$

where μ is the chemical potential of the fluid, F_{ex} and F_{id} are the excess free energy of hard-sphere chains and the ideal free energy, respectively, and F_{att} is the free energy due to attractive forces between particles. $V_{ext}(\mathbf{R})$ is the external potential for a chain molecule assumed to be a sum of the external potential energies imposed on individual segments

$$V_{ext}(\mathbf{R}) = \sum_{j=1}^{M} v_j(\mathbf{r}_j) \; . \tag{6}$$

The configurational ideal part of the free energy functional, F_{id} is known exactly

$$\beta F_{id}[\rho(\mathbf{R})] = \left\{ \beta \int d\mathbf{R}\rho(\mathbf{R})V_b(\mathbf{R}) \; + \int d\mathbf{R}\rho(\mathbf{R}) \ln(\rho(\mathbf{R})) - 1] \right\} \; . \tag{7}$$

Following Yu and Wu[17] we assume that F_{ex} is a functional of average segment density defined as

$$\rho_s(\mathbf{r}) = \sum_{j=1}^{M} \rho_{s,j}(\mathbf{r}) = \sum_{j=1}^{M} \int d\mathbf{R}\delta(\mathbf{r} - \mathbf{r}_j)\rho(\mathbf{R}) \; , \tag{8}$$

where $\rho_{s,j}(\mathbf{r})$ is the local density of the segment j of the chain.

The free energy F_{ex} is a volume integral over free energy density, $F_{ex} = \int \Phi(\mathbf{r})d\mathbf{r}$, and the free energy density can be split into the hard-sphere contribution, $\Phi_{(HS)}$, resulting from the hard-sphere repulsion between segments and the contribution due to the chain connectivity, $\Phi_{(P)}$.

For the hard-sphere contribution we use the following expression, resulting from the fundamental measure theory[32,33,34]

$$\Phi_{(HS)} = -n_0 \ln(1 - n_3) + \frac{n_1 n_2 - \mathbf{n}_1 \cdot \mathbf{n}_2}{1 - n_3} + n_2^3 (1 - \xi^2)^3 \frac{n_3 + (1 - n_3)^2 \ln(1 - n_3)}{36\pi n_3^2 (1 - n_3)^2} \; , \tag{9}$$

where $\xi(\mathbf{r}) = |\mathbf{n}_2(\mathbf{r})|/n_2(\mathbf{r})$.

The contribution $\Phi_{(P)}$ is evaluated using Wertheim's first-order perturbation theory[18]

$$\Phi_{(P)} = \frac{1 - M}{M} n_0 \zeta \ln[y_{(HS)}(\sigma)] \; , \tag{10}$$

where $\zeta = 1 - \mathbf{n}_{V2} \cdot \mathbf{n}_{V2}/(n_2)^2$, with $y_{(HS)}$ given by the Carnahan-Starling expression for the contact value of the radial distribution function of hard spheres is used

$$y_{hs}(\sigma) = \frac{1}{1 - n_3} + \frac{n_2 \sigma \zeta}{4(1 - n_3)^2} + \frac{(n_2 \sigma)^2 \zeta}{72(1 - n_3)^3} \; . \tag{11}$$

with $\zeta = 1 - \mathbf{n}_{V2} \cdot \mathbf{n}_{V2}/(n_2)^2$. In Eqs. [(9)-(11)] the spatial dependence of all variables has been suppressed, for the sake of simplicity. In the above n_α, $\alpha = 0, 1, 2, 3, V1, V2$ denote the weighted densities defined as the spatial convolutions of the average densities and the corresponding weight functions

$$n_\alpha(\mathbf{r}) = \int d\mathbf{r}' \rho_s(\mathbf{r}') w_\alpha(\mathbf{r} - \mathbf{r}') \; , \tag{12}$$

with the weight functions $w_\alpha(\mathbf{r})$ given in Ref.[32].

Finally, the mean-field attractive potential contribution to the free-energy is given by

$$F_{att} = \sum_{j,j'=1,M} \frac{1}{2} \int d\mathbf{r} d\mathbf{r}' u(|\mathbf{r} - \mathbf{r}'|) \rho_{s,j}(\mathbf{r}) \rho_{s,j'}(\mathbf{r}'). \tag{13}$$

If all the segments are identical, Eq. (13) becomes

$$F_{att} = \frac{1}{2} \int d\mathbf{r} d\mathbf{r}' u(|\mathbf{r} - \mathbf{r}'|) \rho_s(\mathbf{r}) \rho_s(\mathbf{r}'). \tag{14}$$

At equilibrium the density profile $\rho(\mathbf{R})$ satisfies the condition $\delta\Omega[\rho(\mathbf{R})]/\delta\rho(\mathbf{R}) = 0$. This condition leads to the equation

$$\rho(\mathbf{R}) = \exp\left\{ \beta\mu - \beta V_b(\mathbf{R}) - \beta \sum_{j=1,M} \lambda_j(\mathbf{r}_j) \right\} \; , \tag{15}$$

where $\lambda_j(\mathbf{r}_j)$ is

$$\lambda_j(\mathbf{r}_j) = \frac{\delta \left[F_{ex} + F_{att} \right]}{\delta \rho_s(\mathbf{r}_j)} + v_j(\mathbf{r}_j). \tag{16}$$

The density profile equation (15) can be combined with Eq. (8) yielding the equation for the average segment local density

$$\rho_s(\mathbf{r}) = \exp(\beta\mu) \int d\mathbf{R} \sum_{j=1}^{M} \delta(\mathbf{r} - \mathbf{r}_j) \exp\left[-\beta V_b(\mathbf{R}) - \beta \sum_{l=1}^{M} \lambda_l(\mathbf{r}_l)\right] . \tag{17}$$

If the density distribution varies only in the z-direction the last equation can be rewritten as

$$\rho_s(z) = \exp(\beta\mu) \sum_{j=1}^{M} \exp[-\beta\lambda_j(z)] G_j(z) G_{M+1-j}(z) , \tag{18}$$

where the propagator function $G_j(z)$ is determined from the recurrence relation

$$G_j(z) = \int dz' \exp[-\beta\lambda_j(z')] \frac{\theta(\sigma - |z - z'|)}{2\sigma} G_{j-1}(z') \tag{19}$$

for $j = 2, 3, \ldots, M$ and with $G_1(z) \equiv 1$.

III. RESULTS AND DISCUSSION

We have studied adsorption of chains composed of $M = 2$, 4, 6, 8 and 10 segments. Prior to surface studies, we have evaluated the bulk phase diagrams using the theory outlined in the preceding section with the local density being constant and equal to the bulk density, ρ_b. In a homogeneous system the vector weighted densities vanish, while the scalar weighted densities become proportional to the bulk density. From Eq. (12) we obtain $n_\alpha = \xi_\alpha M \rho_b = \xi_\alpha \rho_{s,b}$, with $\xi_3 = (\sigma)^3\pi/6$, $\xi_2 = (\sigma)^2\pi$, $\xi_1 = \sigma/2$ and $\xi_0 = 1$. Insertion of the bulk weighted densities defined above into Eqs. (9)-(11) together with Eq. (7) leads to the total free energy per unit volume, from which the pressure and the chemical potential can be readily obtained. The bulk phase diagrams were obtained from the condition that at the coexistence the chemical potentials and the pressures of a fluid in the liquid and vapor phases are equal. As pointed out in Ref.[2], Wertheim thermodynamic perturbation theory does not accurately describe the gas phase but it relatively well accounts for the properties of a liquid phase of provided that the system is well removed from the critical region.

In Fig. 1 we show examples of the liquid-vapor coexistence envelopes in the reduced segment density $\rho_b^* = \rho_{s,b}\sigma^3$ – reduced temperature $T^* = k_B T/\varepsilon$ plane for several values of the chain length M. Although the surface calculations have been carried out for $M \leq 10$, the result for $M = 16$ is also included here. Diamonds mark the critical points for all the chains lengths from $M = 2$ up to $M = 16$. For $2 <\leq M \leq 10$ the critical temperatures can be approximated by $T^{*,cr} = 0.75764 + 0.95646\ln(M)$. The corresponding correlation coefficient is high and equals 0.99948. Moreover, the critical densities can be approximated by $\rho_{s,b}^{cr} = 0.26376 M^{-0.38252}$ with the correlation coefficient equal -0.99955. The knowledge of bulk phase diagrams is necessary for the studies of adsorption from gaseous bulk phase at temperatures lower than the bulk critical temperature.

We begin with the presentation of the results obtained for $\varepsilon_{gs}/\varepsilon = 6$. For a given value of M we first solve the density profile equation (18) and then evaluate the "segment adsorption isotherm"

$$\Gamma = \int_0^\infty dz[\rho_s(z) - \rho_{s,b}] \tag{20}$$

and the excess grand potentials $\Delta\Omega = \Omega - \Omega_b$, where Ω_b is the grand potential of an uniform fluid being in equilibrium with the nonuniform system. The analysis of the dependence of $\Delta\Omega$ on the chemical potential allows us for a precise location of the surface phase transitions. Note that the form of the external potential Eq. 3 implies that the resulting wetting transition is first order[35,36].

In figure 2 we show examples of the adsorption isotherms, obtained for $M = 8$ at two temperatures. The first of them, $T^* = 1.1$ (cf. Fig. 2a) is somewhat higher than the wetting temperature. For the system in question the latter temperature is approximately equal to $T_w^* \approx 0.845$. The adsorption isotherm in Fig. 2a exhibits a well-pronounced prewetting jump. This jump occurs at the bulk density significantly lower than the segment density at bulk coexistence. Instantaneously, the adsorption before the jump is very low. Indeed, it is almost zero on the figure scale.

With the temperature increase the prewetting jump becomes smaller, see Fig. 2b where we have plotted the isotherm evaluated at $T^* = 1.85$. This temperature is close to the surface critical temperature, which for the investigated system equals to $T_{sc}^* \approx 1.965$. We have also shown here the metastable branches of the isotherm. The equilibrium transition is marked by dashed line.

Figure 3 shows representative examples of the average segment density profiles, calculated for the systems from Fig. 2. Profiles in Fig. 3a have been evaluated at $T^* = 1.1$ for the bulk fluid densities lower (dashed lines) and higher (solid line) than the density at the prewetting jump. Dotted line marks the bulk segment density for the corresponding liquid phase. The profile at the bulk density lower than the density at the prewetting transition is extremely low (the relevant curve in Fig. 3a has been multiplied by 500) and extends over approximately one layer. After the prewetting a thick film exhibiting a well-pronounced layered structure and extending over approximately 6 monomer layers is developed. The film thickness is lower than the chain length and the consecutive maxima of the profile are at a distance approximately equal to σ. Similar thick film morphology is found in simple fluids, however in the chain fluid considered here the first peak is relatively smaller.

Figure 3b illustrates the film growth after the prewetting transition at $T^* = 1.85$. Note that, contrary to Fig. 3a, the profile before the transition (dashed line) has not been magnified. This is reflected in the smaller jump on the corresponding adsorption isotherm (cf. Fig. 2b). Directly after this transition, the surface film extends over approximately three layers. At the bulk density close to the bulk coexistence the film thickness grows rapidly, and at the highest density displayed in Fig. 3b spans approximately 18 monomer layers. The layered structure of the film is less pronounced than at $T^* = 1.1$. Indeed, only three consecutive maxima on the profiles are observed. At distances from the surface larger than 4σ the thick film exhibits a plateau within which the adsorbed fluid segment density is close to the bulk liquid density at the bulk gas-liquid coexistence.

Figure 4 gives a further insight into the film growth. We find that at both temperatures, $T^* = 1.1$ (Fig. 4a) and $T* = 1.85$ (Fig. 4b) the adsorption divergence upon approaching coexistence is a power law i.e. $\Gamma^* \propto (\rho^*_{b,c} - \rho^*_b)^{-1/3}$, where $\rho_{b,c}$ is the gas segment density at bulk coexistence. This behavior is clearly visible on the log-log plot of adsorption where the straight line slope equals -1/3. The same behavior has been observed for all the systems under study and is characteristic for the complete wetting regime in systems with long-range fluid-fluid and/or fluids-solid potentials[36].

Within the present approach it is possible to track down the density profiles of particular segments of a chain molecule. The segment local densities provide an additional insight into the structure of adsorbed fluid. In Fig. 5 we show representative examples of the end ($j = 1$ or, equivalently $j = 8$) and middle ($j = 4$ or, equivalently $j = 5$) segment local densities obtained for $M = 8$ at $T^* = 1.1$ (part a) and at $T^* = 1.85$ (part b). These plots correspond to the systems from Fig. 2. At lower temperature (cf. Fig. 5a) the shape of the end and middle segment profiles is almost identical before the prewetting transition due to the fact that the density is very low (the profiles were multiplied by 500). After the prewetting transition we find that the consecutive maxima of both profiles are at almost the same distances from the surface but the first local density maximum of the end segments is higher than that of the middle segments. End segments seem to be more "pinned" to the surface. These findings are in accordance with results of Monte Carlo simulations and self consistent field theory[25]. We also note that the structure of the tails of the profiles is similar to that observed previously in the case of a fluid-fluid interface of a mixture of polymers built of tangentially jointed hard spheres[20].

Examples of the surface phase diagrams evaluated for dimers (part a) and 8-mers (part b) are plotted in Fig. 6. Similar to the case of simple fluids the prewetting line (solid line) joins the binodal (dashed line) tangentially in a wetting point (open triangle) and ends at the surface critical point (open circle). The reduced wetting temperature T^*_w and the surface critical temperature T^*_{sc} increases with an increase of the chain length. However, since the bulk critical temperature increases as well, it is convenient to re-scale (divide) both T^*_w and T^*_{sc} by T^*_c. In Fig. 7 where we display the rescaled wetting temperature, $t^*_w \equiv T^*_w/T^*_c$, and the rescaled surface critical temperature $t^*_{sc} \equiv T^*_{sc}/T^*_c$, for $M = 2$, 4, 6, 8 and 10. All the calculations were carried out for $\varepsilon_{gs}/\varepsilon = 6$. For a better visualization of the occurring changes we also plot here the bulk critical temperatures (marked on the right-hand side y-axis). The increase of the chain length leads to a decrease of $t^*_w \equiv T^*_w/T^*_c$ and to an increase of $t^*_{sc} \equiv T^*_{sc}/T^*_c$. For $M \geq 8$ the both t^*_w and t^*_{sc} attain plateau. This information may be useful in finding a quick estimate of the wetting or surface critical temperatures for fluids composed of longer chain lengths.

Finally, we address briefly the issue of the surface wettability changes with change of the strength of the segment-surface potential, ε_{gs}. Figure 8 presents the plot of the dependence of T^*_w and T^*_{sc} on $\varepsilon^*_{gs} = \varepsilon_{gs}/\varepsilon$ for the chains of the length $M = 4$. When ε^*_{gs} decreases both characteristic surface temperatures increase and the gap between them becomes smaller, as expected. For $\varepsilon^*_{gs} = 2$ the surface critical temperature $T^*_{sc} \approx 2.01$ becomes only marginally higher than the wetting temperature, $T^*_w \approx 2.03$ and both these temperatures become only slightly lower than the corresponding bulk critical temperature. Extrapolation of the obtained results suggest that the line of the wetting points (triangles) would cross $T^*_w = T^*_c$ for $\varepsilon^*_{gs} \approx 1.8$. However such decrease of ε^*_{gs} would lead to a crossover from a complete wetting regime to a critical adsorption regime. Since in our studies we employ a simple mean-field functional we have not performed the relevant calculations here and leave this issue for a more elaborated approach. On the other hand, an increase of ε_{gs} would lead to a decrease of both T^*_{sc} and T^*_w temperatures. One can also expect the occurrence of layering-type transitions at high values of ε^*_{gs} and at low temperatures. We have not explored the layering transitions in the present work. The relevant results will be presented in a future.

IV. SUMMARY

We have carried out studies of wetting behavior of fluids composed of chains built of freely jointed tangent Lennard-Jones monomers. The difference in the chain lengths leads to the difference in the wetting behavior. We have found that the wetting temperatures rescaled by the bulk critical temperature decrease with an increase of the chain length. For higher values of M the observed decrease becomes smaller and the curve of the chain length dependence of the rescaled wetting temperature, $t_w^*(M)$ attains a plateau for $M \geq 9$. In the case of the chain length dependence of the rescaled surface critical temperatures, $t_{sc}^*(M)$ an inverse effect has been observed, i.e. this temperature increases with the chain length and then attains a plateau for $M \geq 9$. We have also found that the thick film diverges according to the power law $\Gamma \propto (\rho_{bc} - \rho_b)^{-1/3}$) in accordance with the general predictions for the fluids interacting with long range forces[36]. The theory allows for a detailed investigation of the adsorbed fluid structure. Our analysis has revealed that the end segments adsorb preferentially in the first adsorbed layer which is in qualitative agreement with the results of Monte Carlo simulations and self consistent field theory[25].

It would be of interest to check our predictions against computer simulations. However such task would require rather long-lasting calculations, and we postpone such studies for a future. Our study cannot be considered as complete because we have not discussed the layering transitions transition. However, ascertaining the global surface phase diagrams for a system of freely jointed Lennard-Jones chains poses many difficulties and we postpone systematic investigations of this issue for further works.

Acknowledgments

P.B. acknowledges financial support from the Rector of the Maria Curie-Skłodowska University, Lublin. S.S. acknowledges EU for a partially funding this work as a TOK contract 509249.

---

[1] A. Milchev, in *Computational Methods in Colloid and Surface Science*, ed. M. Borówko, Marcel Dekker, New York 2000, ch. 12.
[2] M. Müller and L.G. McDowell, J. Phys.: Condens. Matter **15**, R609 (2003).
[3] P. Smith, R.M. Lynden-Bell, and W. Smith, Molec. Phys. **98**, 255 (2000).
[4] S. Balasubramanian, M.L. Klein, and J.I. Siepmann, J. Chem. Phys. **103**, 3184 (1995).
[5] L.J.M. Schlangen and L.K. Koopal, Langmuir **12**, 1863 (1996).
[6] L.J.M. Schlangen, F.A.M. Leermakers, and L.K. Koopal, J. Chem. Soc. Faraday Trans **92**, 579 (1996).
[7] M.B. Sweatman, J. Phys.: Condens. Matter **15**, 3875 (2003).
[8] C.E. Woodward, J. Chem. Phys. **94**, 3138 (1991).
[9] C.E. Woodward, J. Chem. Phys. **97**, 4525 (1992).
[10] A. Yethiraj and C.E. Woodward, J. Chem. Phys. **102**, 5499 (1995).
[11] A. Yethiraj, J. Chem. Phys. **109**, 3269 (1998).
[12] D. Chandler, J.D. McCoy, and S.J. Singer, J. Chem. Phys. **85**, 5971 (1986).
[13] J.B. Hooper, J.D. McCoy, and J.G. Curro, J. Chem. Phys. **112**, 3090 (2000).
[14] S.K. Nath, P.F. Nealey, and J.J. de Pablo, J. Chem. Phys. **1120**, 7483 (1999).
[15] A. L. Frischknecht, J.G. Curro, and L.J.D. Frink, J. Chem. Phys. **117**, 10398 (2002).
[16] E. Kierlik and M.L. Rosinberg, J. Chem. Phys. **97**, 9222 (1992).
[17] Y.-X. Yu and J. Wu, J. Chem. Phys. **117**, 2368 (2002).
[18] M.S. Wertheim, J. Chem. Phys. **87**, 7323 (1987).
[19] Y.-X. Yu and J. Wu, J. Chem. Phys. **118**, 3835 (2003).
[20] P. Bryk and S. Sokołowski, J. Chem. Phys. **120**, 8299 (2004).
[21] C.N. Patra and A. Yethiraj, J. Chem. Phys. **112**, 1579 (2000).
[22] C.N. Patra and A. Yethiraj, J. Chem. Phys. **118**, 4702 (2003).
[23] M. Müller and L.G. MacDowell, Macromolecules **33**, 3902 (2000).
[24] M. Müller, L.G. MacDowell, P. Müller-Buschbaum, O. Wunnike, and M. Stamm, J. Chem. Phys. **115**, 9960 (2001).
[25] M. Müller, L.G. MacDowell and A. Yethiraj, J. Chem. Phys. **118**, 2929 (2003).
[26] S. Zhang, J. Cai, H. Liu, and Y. Hu, Molec. Simulat. **30**, 143 (2004).
[27] A. Gil-Villegas, A. Galindo, P.J. Whitehead, S.J. Mills, and G. Jackson, J. Chem. Phys. **106**, 4168 (1997).
[28] L.G. MacDowell, M. Müller, C. Vega, and K. Binder, J. Chem. Phys. **113**, 419 (2000).
[29] Y.P. Lee, G.P. Rangaiah, and Y.C. Chiew, Fluid Phase Equil. **189**, 135 (2001).
[30] J.C. Pámies and L.F. Vega, Molec. Phys. **100**, 2519 (2002).

[31] X.-Y. Wang and Y.C. CHiew, J. Chem. Phys. **115**, 4376 (2001).
[32] Y. Rosenfeld, Phys. Rev. Lett. **63**, 980 (1989).
[33] R. Roth, R. Evans, A. Lang, and G. Kahl, J. Phys.: Condens. Matter **14**, 12063 (2002).
[34] Y.-X. Yu and J. Wu, J. Chem. Phys. **117**, 10165 (2002).
[35] S. Dietrich, in *Phase Transitions and Critical Phenomena*, ed. C. Domb and J.L. Lebowitz, Academic, London, 1988, Vol. 12, p. 1.
[36] D.E. Sullivan and M.M. Telo da Gama, in *Fluid Interfacial Phenomena*, ed. C.A. Croxton, Wiley, New York, 1986, p. 45.

Figure Captions

Fig. 1. Bulk phase diagrams (binodals) of tangentially jointed Lennard-Jones chains, characterized by different number of beads $M = 2, 4, 8, 16$ evaluated in the reduced bulk segment density ρ_b^* – reduced temperature T^* representation. Open diamonds indicate the locations of the critical points for chains with $2 \leq M \leq 16$. The reduced units are defined as: $\rho_b^* = \rho_{s,b}\sigma^3$ and $T^* = k_B T/\varepsilon$.

Fig. 2. Segment adsorption isotherms of tangentally jointed Lennard-Jones 8-mers adsorbed on a solid planar surface with $\varepsilon_{gs}^* = 6$ plotted as a function of a relative undersaturation $\rho_b^* - \rho_{b,c}^*$ evaluated at two reduced temperatures: $T^* = 1.1$ (part a), and $T^* = 1.85$ (part b). Dashed line in part b marks the equilibrium prewetting transition.

Fig. 3. (a) Average segment density profiles of tangentially jointed Lennard-Jones 8-mers before (dashed line, $\rho_b^* = 2.0244243 \times 10^{-07}$) and after (solid line, $\rho_b^* = 2.0244424 \times 10^{-07}$) the prewetting transition evaluated for $T^* = 1.1$. The dashed profile was multiplied by 500. (b) Average segment density profiles of tangentially jointed Lennard-Jones 8-mers before (dashed line, $\rho_b^* = 0.0015$) and after (solid lines, from left to right for $\rho_b^* = 0.0016, 0.0017, 0.0018, 0.0019, 0.0020, 0.0021, 0.00215$, and 0.002156, respectively) the prewetting transition evaluated for $T^* = 1.85$. Dotted line in both figures marks bulk segment density of the liquid phase.

Fig. 4. Segment adsorption isotherms of tangentially jointed Lennard-Jones 8-mers adsorbed on a solid planar surface with $\varepsilon_{gs}^* = 6$ (circles) plotted as a function of the logarithm of the deviation from bulk coexistence $\log(\rho_b^* - \rho_{b,c}^*)$ evaluated at two reduced temperatures: $T^* = 1.1$ (part a), and $T^* = 1.85$ (part b). Solid line in both parts has a slope -1/3.

Fig. 5. (a) Middle (solid lines) and end (dashed lines) segment density profiles of tangentially jointed Lennard-Jones 8-mers before ($\rho_b^* = 2.0244243 \times 10^{-07}$) and after ($\rho_b^* = 2.0244424 \times 10^{-07}$) the prewetting transition evaluated for $T^* = 1.1$. The profiles before the prewetting transition were multiplied by 500. (b) Middle (solid lines) and end (dashed lines) segment density profiles of tangentially jointed Lennard-Jones 8-mers evaluated for $T^* = 1.85$ and for $\rho_b^* = 0.00215$.

Fig. 6. The surface phase diagrams of tangentially jointed Lennard-Jones dimers (a) and 8-mers (b) plotted in the reduced bulk density – reduced temperature representation. Shown are the prewetting lines (solid lines), the gas branch of the corresponding bulk phase diagrams (dashed lines), the bulk critical points (filled circles), the surface critical points (open circles) and the wetting points (open triangles). The corresponding temperatures are marked in the Figure.

Fig. 7 The dependence of the reduced bulk critical temperature T_c^* (filled circles), the rescaled surface critical temperature T_{sc}^*/T_c^* (open circles), and the rescaled wetting temperature T_w^*/T_c^* (open triangles) on the chain length M. Dotted and dashed lines serve as a guide to the eye. Arrows point to the relevant temperature axis.

Fig. 8 The dependence of the reduced surface critical temperature T_{sc}^* (open circles), and the reduced wetting temperature T_w^* (open triangles) on the reduced segment-surface energy parameter ε_{gs}^* evaluated for the constant chain length $M = 4$.

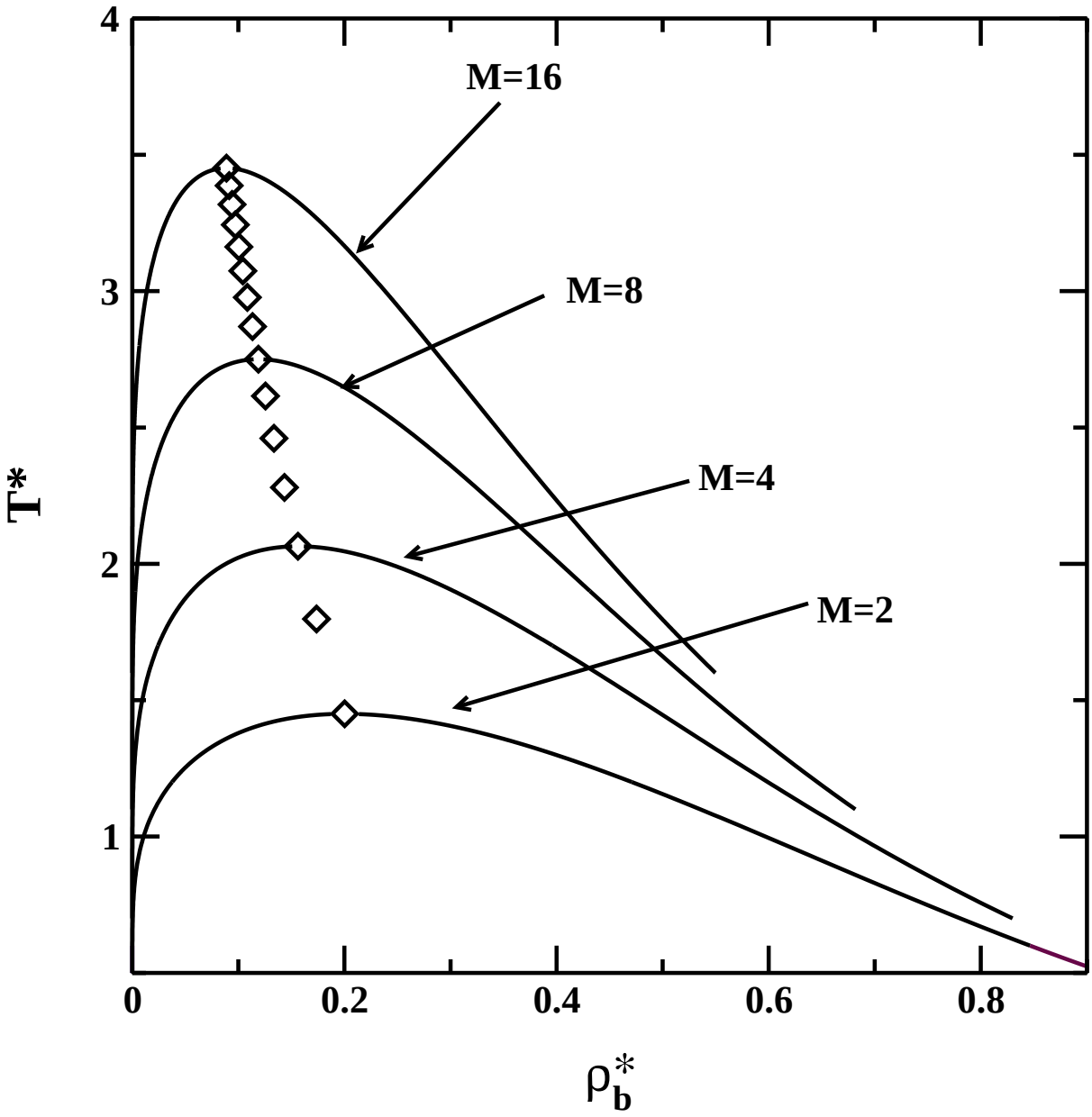


FIG. 1:

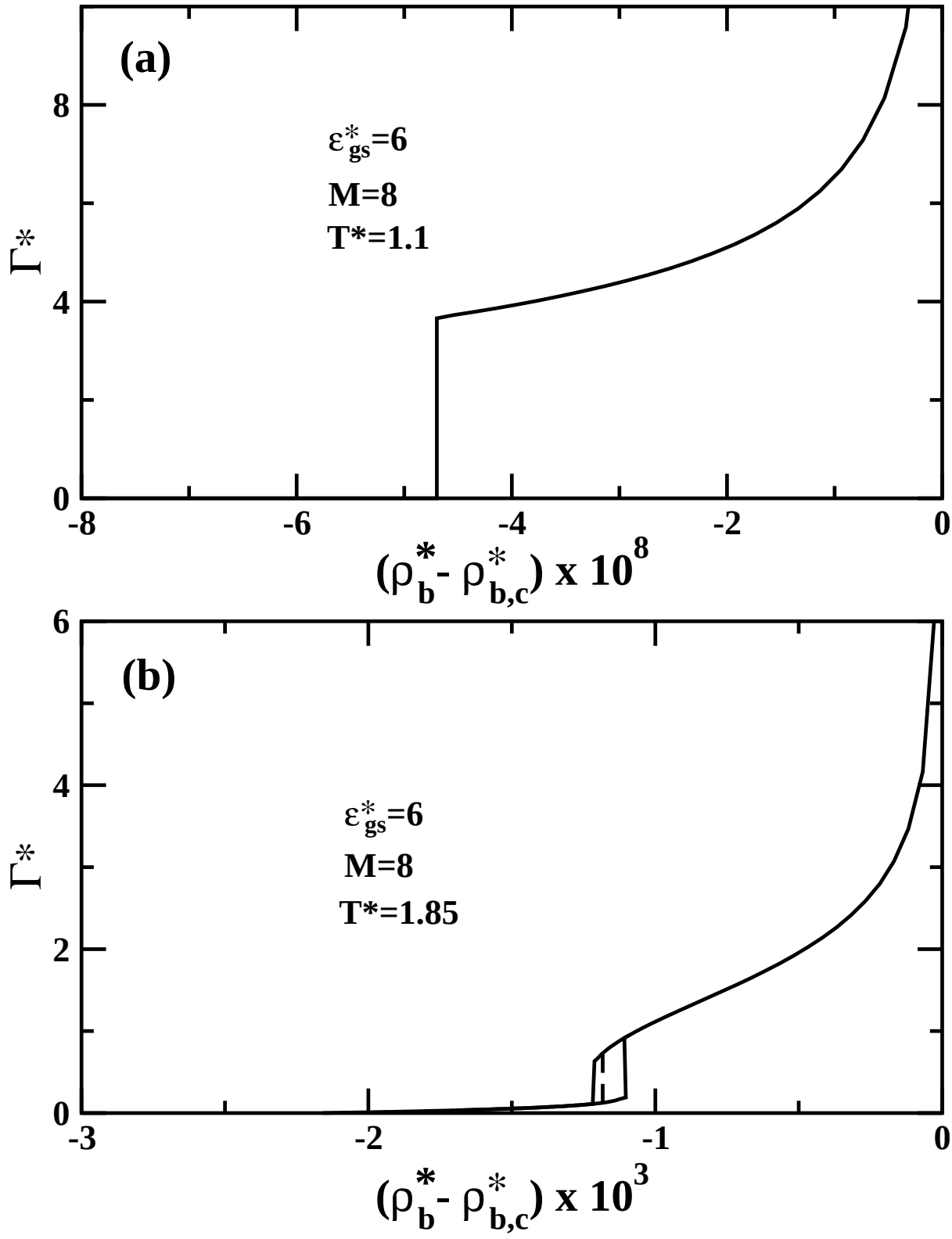

(a)
ε^*_{gs}=6
M=8
T*=1.1
Γ^*
0
4
8
-8
-6
-4
-2
0
$(\rho^*_b - \rho^*_{b,c}) \times 10^8$
(b)
ε^*_{gs}=6
M=8
T*=1.85
Γ^*
0
2
4
6
-3
-2
-1
0
$(\rho^*_b - \rho^*_{b,c}) \times 10^3$

FIG. 2:

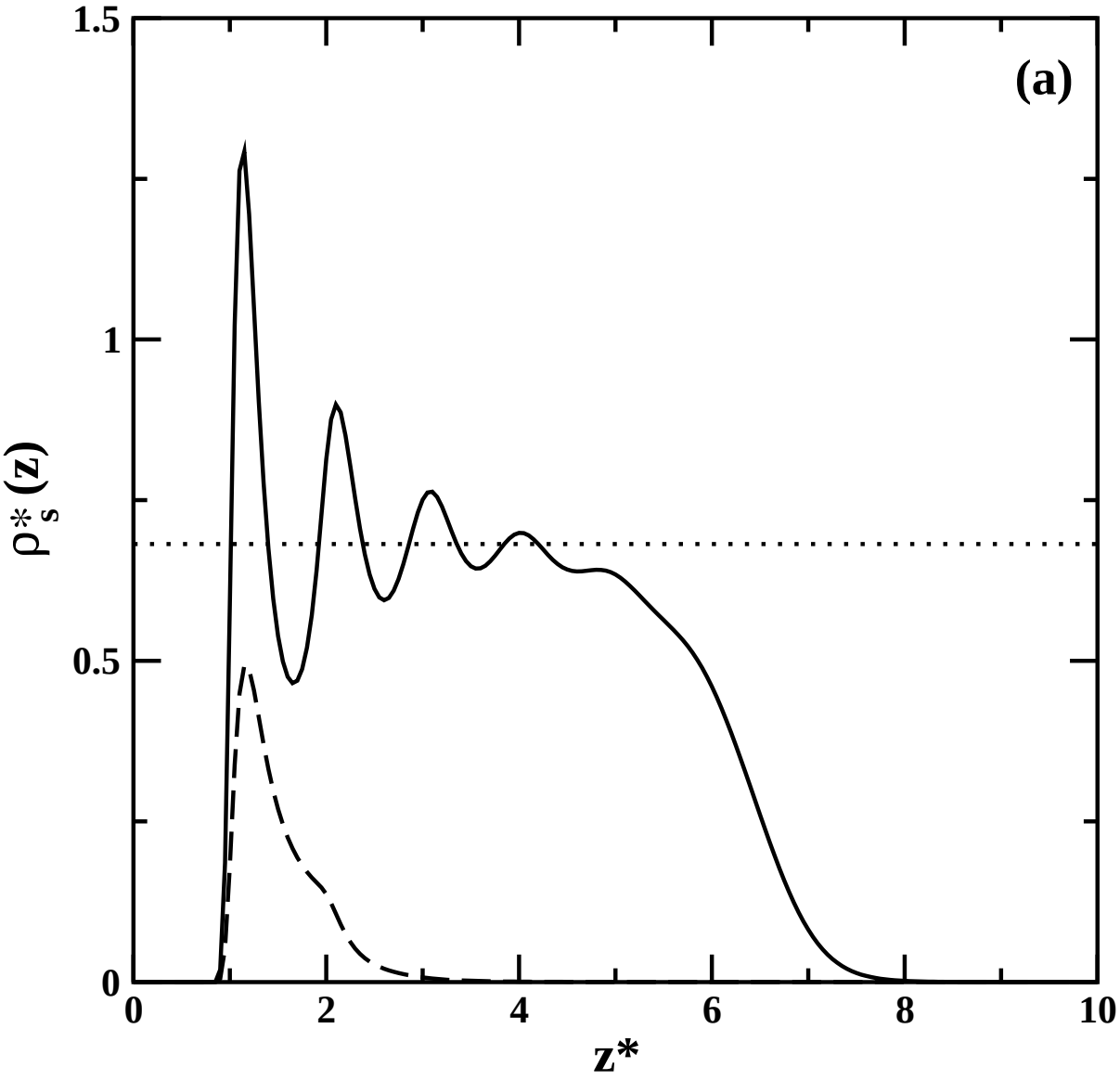
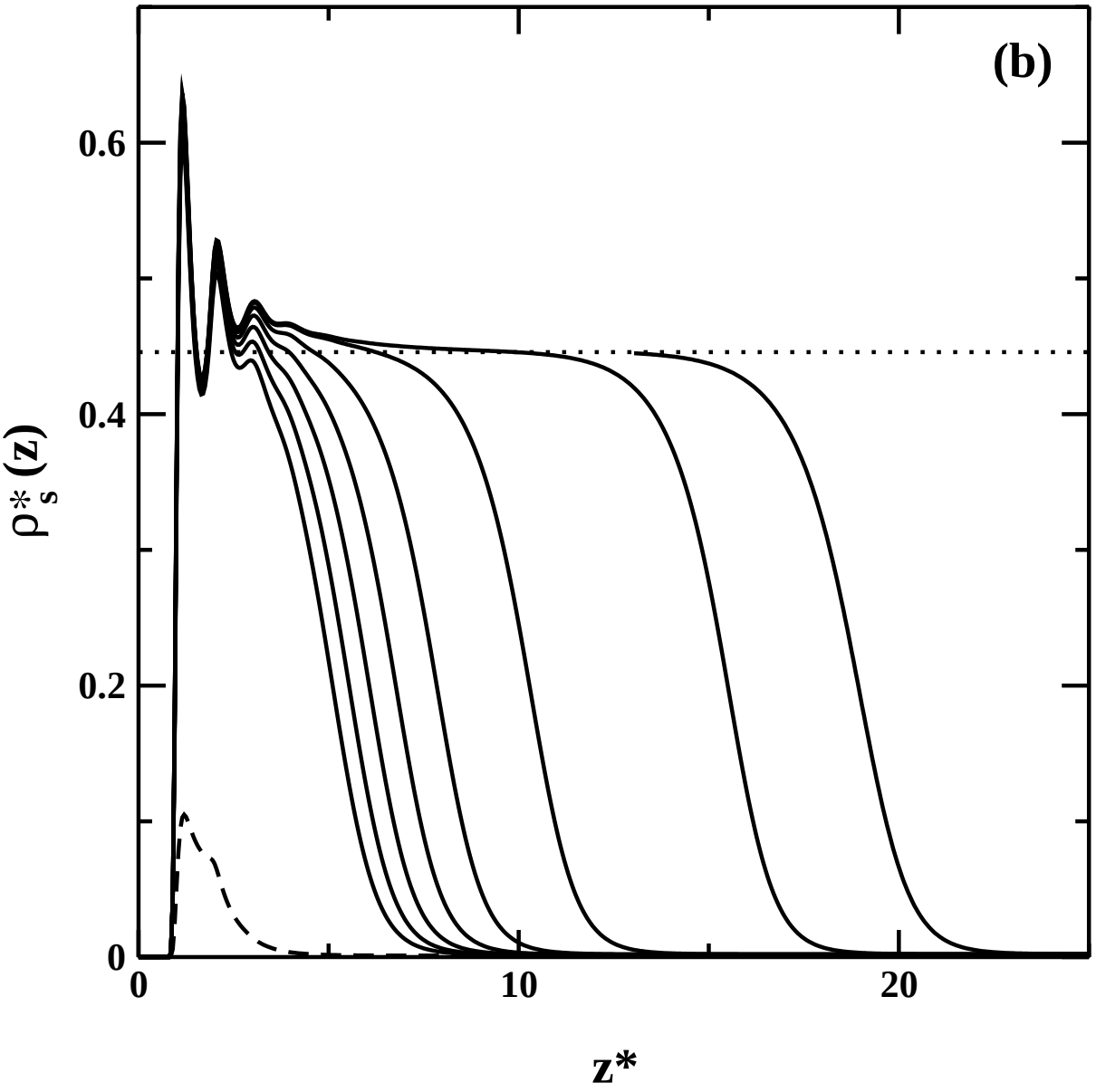


FIG. 3:


(b)
0.6
0.4
0.2
0
0
10
20
ρ*s (z)
z*

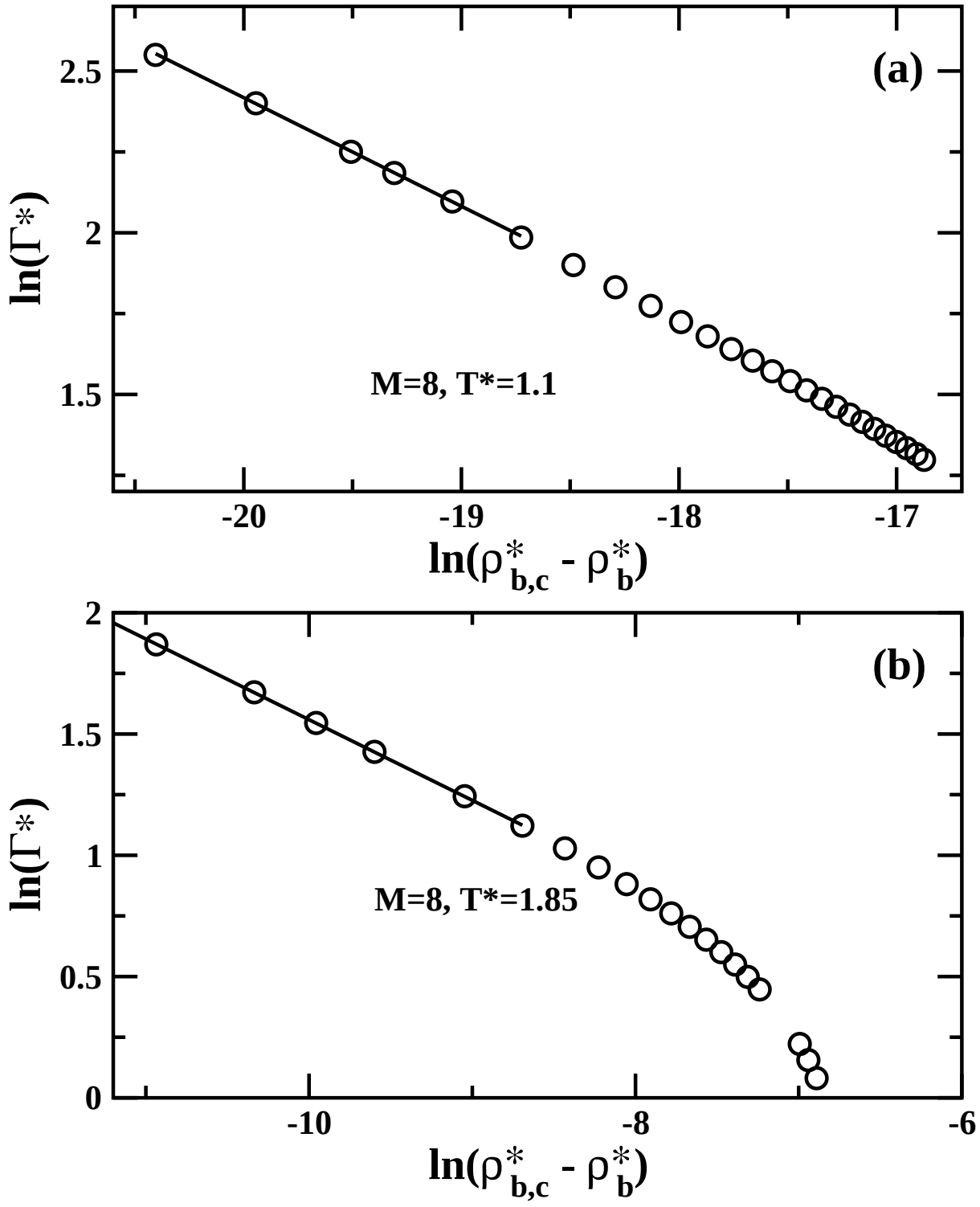

(a)
M=8, T*=1.1
ln(Γ*)
ln(ρ*b,c - ρ*b)
2.5
2
1.5
-20
-19
-18
-17
(b)
M=8, T*=1.85
ln(Γ*)
ln(ρ*b,c - ρ*b)
2
1.5
1
0.5
0
-10
-8
-6

FIG. 4:

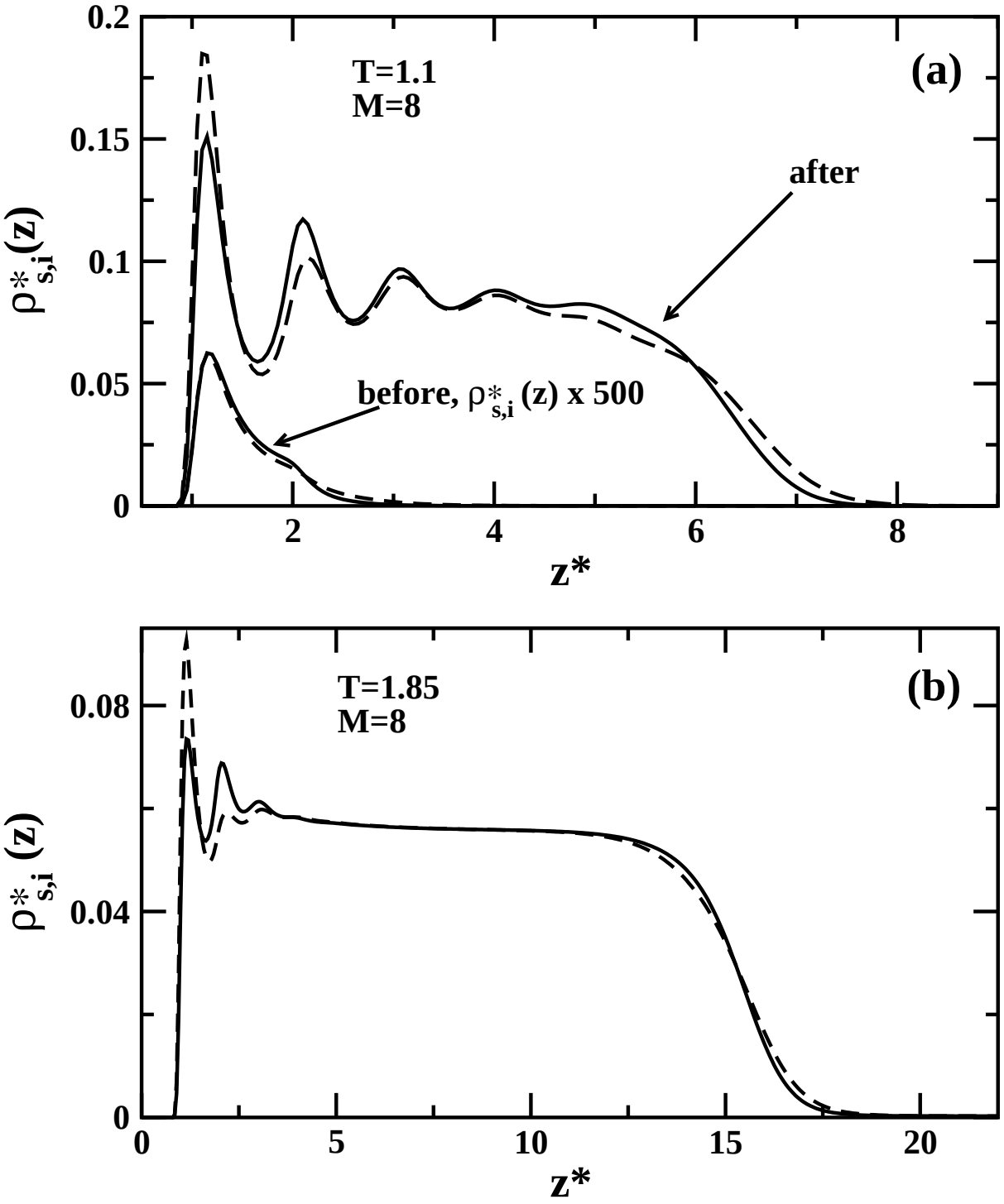

T=1.1
M=8
(a)
after
before, ρ*s,i (z) x 500
ρ*s,i(z)
z*
0.2
0.15
0.1
0.05
0
2
4
6
8
T=1.85
M=8
(b)
ρ*s,i (z)
z*
0.08
0.04
0
0
5
10
15
20

FIG. 5:

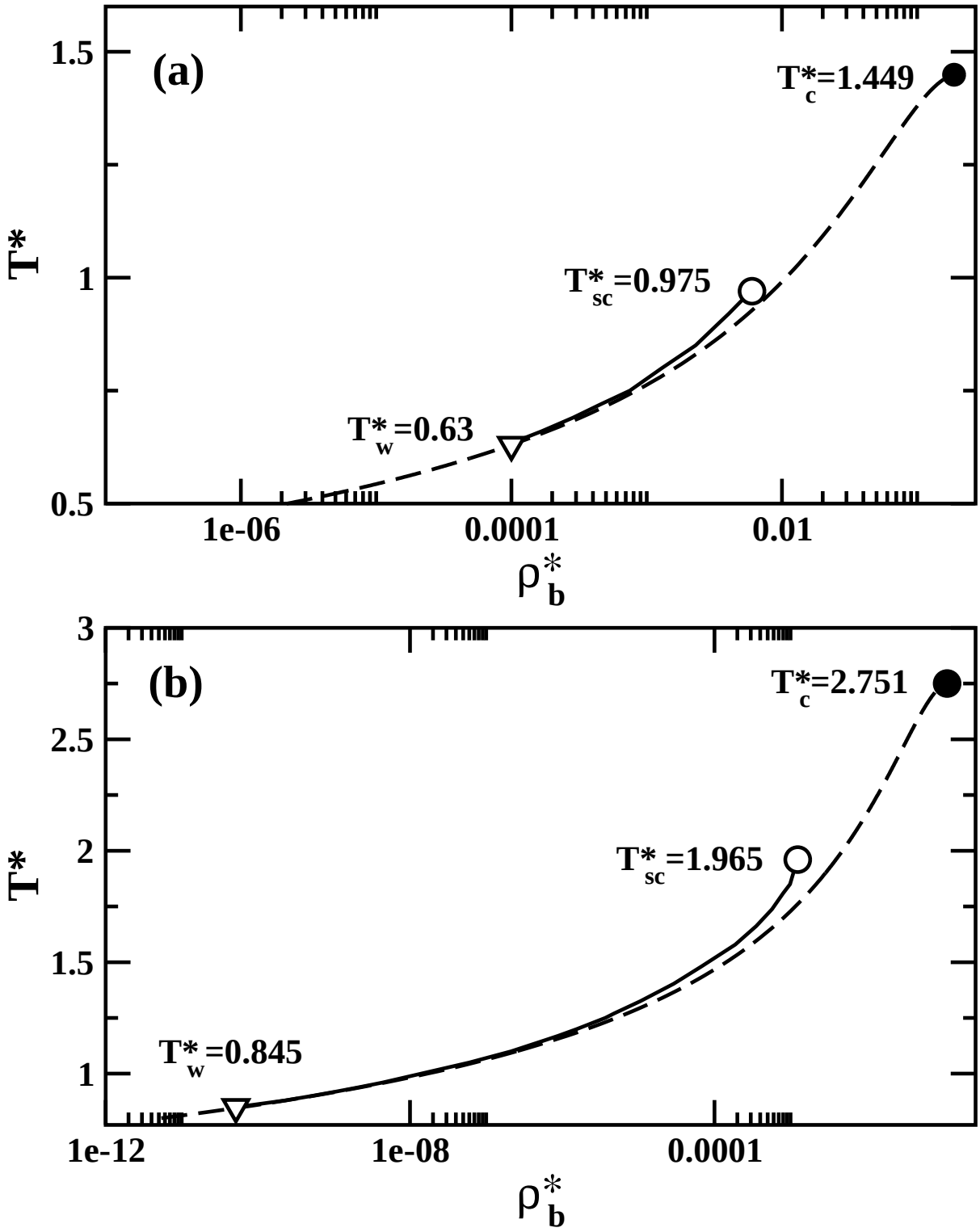

(a)
T*
1.5
1
0.5
T*c=1.449
T*sc=0.975
T*w=0.63
1e-06
0.0001
0.01
ρ*b
(b)
T*
3
2.5
2
1.5
1
T*c=2.751
T*sc=1.965
T*w=0.845
1e-12
1e-08
0.0001
ρ*b

FIG. 6:

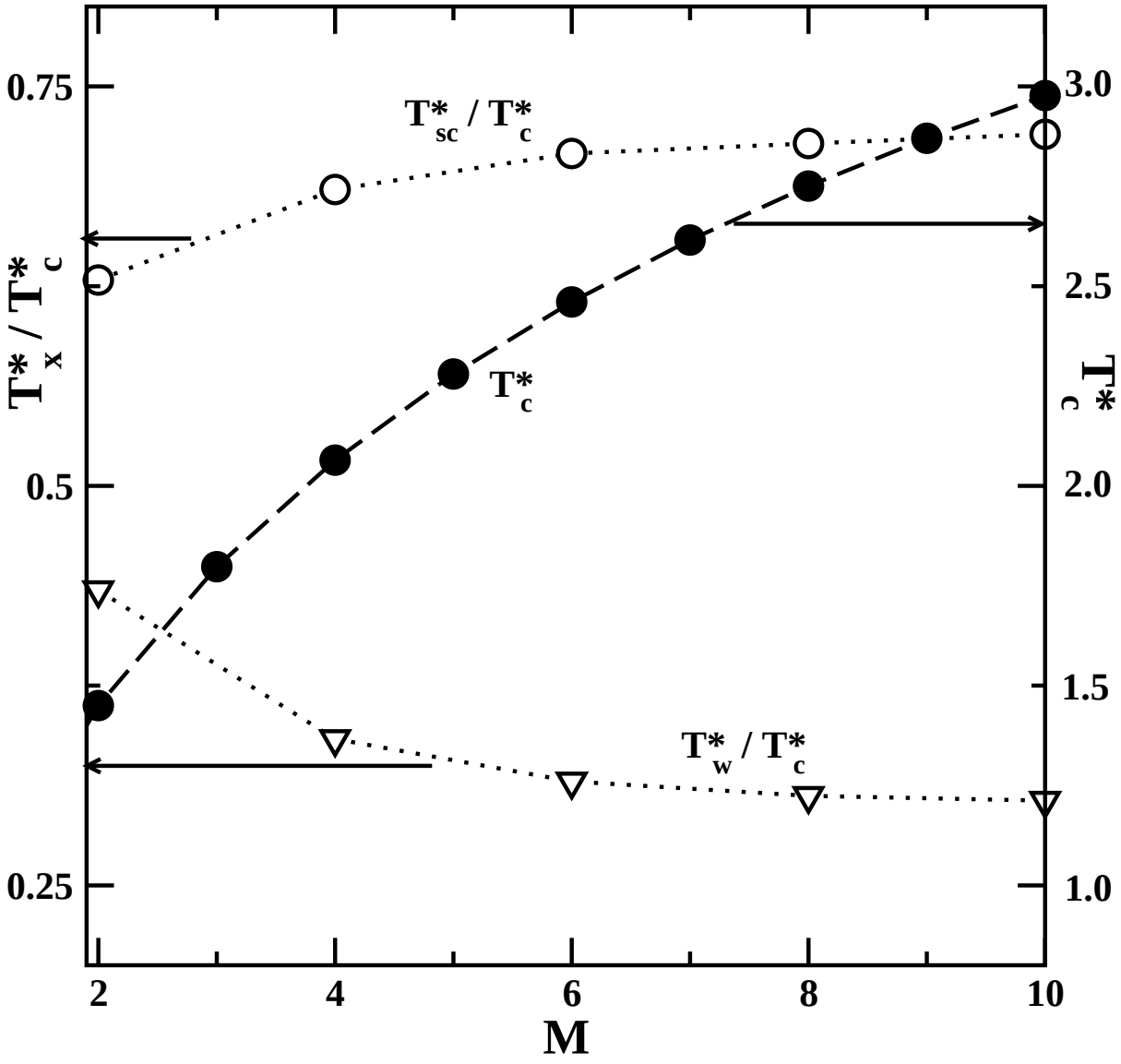


FIG. 7:

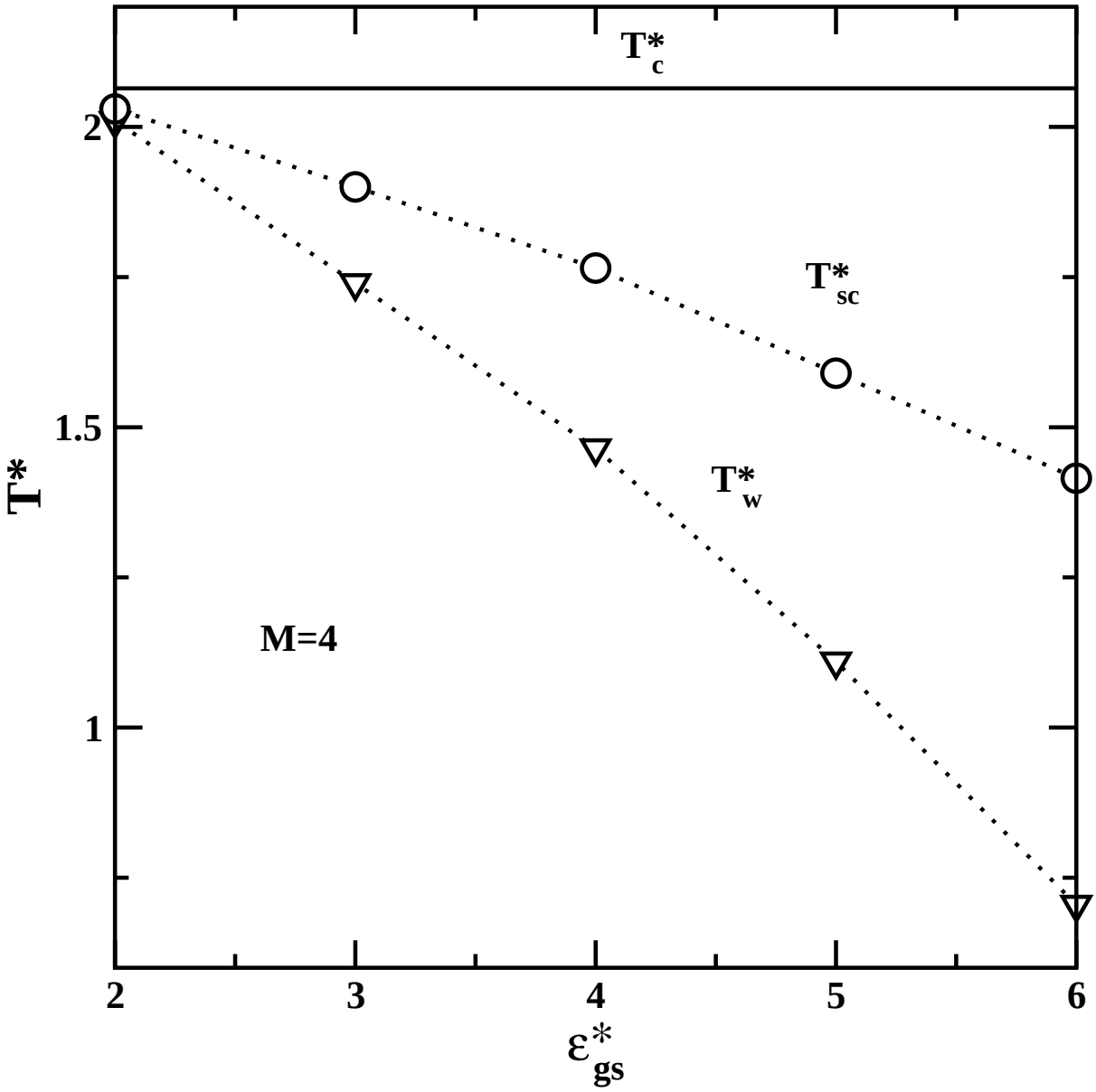


FIG. 8: